scientific reports

Check for updates

OPEN

Miniaturized circularly polarized wearable array antenna for medical device applications

Muammer Omran, Changiz Ghobadi✉, Javad Nourinia & Majid Shokri

Antenna miniaturization is essential for healthcare applications, and numerous studies have tackled the challenge of presenting miniaturized, reliable designs while maintaining performance. This paper presents a small circularly polarized (CP) sequential wearable array antenna with overall dimensions of only 110 mm × 95 mm × 1.8 mm. It comprises four novel designs of circular-shaped elements arranged sequentially in an array configuration measured only 24 mm×24 mm×1 mm. It is fed by a separate cascade feeding network incorporating a single rat-race and two branch-line couplers. The antenna is designed for medical device applications within the 2.4 GHz Industrial Scientific Medical (ISM) frequency band. The proposed design is fabricated and experimentally tested, demonstrating wide impedance bandwidths of 21.24% (2.2–2.72 GHz) and an Axial Ratio (AR) bandwidth (AR < 3 dB) covering the entire 2.4 GHz ISM frequency band. At 2.43 GHz, the antenna achieves a gain of -14.9 dBi. Both simulation and experimental results confirm excellent performance in impedance matching, gain pattern, and circular polarization, making it promising for wearable wireless communication in medical applications. The link margin was calculated, and the specific absorption rate of the antenna was analyzed, the result revealing that it aligns with the safety limits of IEEE C95.1-1999 standards.

Keywords Array antenna, ISM band, Sequential-phase feed network, Medical application, Patch antenna, Circular polarization

Rapid advances in communication and electronics technology have led to increased production and improvement of medical devices in healthcare measurement and monitoring of vital signs, and even therapeutic purposes using highly advanced equipment[1]. Accordingly, different antenna types and designs have appeared in medical device applications.

Generally, medical devices are classified into three categories: wearable, implantable, and ingestible. Over the past few decades, many antenna designs for each medical device category have been proposed[2]. The primary challenge in the antenna design process was decreasing the antenna size while enhancing its efficiency within the permissible frequency range for medical devices[3].

High-gain antennas are indispensable in many applications, encompassing telecommunications, radar systems, and emerging technologies like the Internet of Things (IoT). Reflect arrays, which combine the properties of reflectors and arrays, offer high-gain and beam-steering capabilities. A 1-bit reconfigurable reflect array utilizes simple electronic components to alter the reflection phase of individual elements, thereby adjusting the beam direction. Phased arrays composed of a grid of antenna elements with phase shifters enable precise control over the signal phase at each antenna element. Arrays based on p-i-n diodes are particularly notable for their ability to scan beams dynamically across various angles. Intelligent metasurface-based antennas employ engineered surfaces to manipulate electromagnetic waves innovatively, featuring sub-wavelength elements that can be individually controlled to reconfigure the radiation pattern and beam direction.

Wearable antennas show great potential for various medical applications, offering wireless connectivity and improved performance[4]. There has been considerable interest in developing wearable antennas over the past decade because utilizing these varieties of antennas has the potential to enhance the transmission of signals between a device on a patient body and a remote base station and increase data throughput, making them more viable and reliable in medical devices, this can lead to better healthcare and monitoring of the patient's condition without causing any discomfort[5,6]. This can lead to better health care and monitoring of the patient's condition without causing any inconvenience.

These antennas are designed to operate in the Industrial, Scientific, Medical (ISM), and Medical Body Area Network (MBAN) frequency bands. These frequency bands provide wide functional bandwidth and meet the

Department of Electrical Engineering, Urmia University, Urmia, Iran. ✉email: ch.ghobadi@urmia.ac.ir

specific needs of healthcare monitoring and diagnostics. The resonant frequency and radiation efficiency of the antenna are determined by the thickness of the substrate and its relative electrical permittivity.

Wearable antennas used on printed circuit boards are designed on rigid substrates to facilitate integration with the electronics. Conversely, antennas intended for biomedical applications are often made with flexible substrates to enable easy deployment on living subjects. In WBANs, the choice between rigid and flexible antennas depends on specific application requirements. Rigid antennas offer durability and stable performance for applications where flexibility is not critical, particularly in cases where the antenna size is minimized. Flexible antennas provide the adaptability and comfort necessary for body-centric wireless communications. Both types have their challenges and benefits, and advancements in materials and design techniques continue to enhance their performance and usability in healthcare and wearable technology applications[7–11].

Recent research has introduced wearable antenna designs employing diverse techniques to enhance performance and ensure consistent functionality under different operational conditions[12]. These advancements include improving material properties, expanding bandwidth, and developing multi-band antennas. The presented works encompass single, MIMO, and array antennas, including single-band, dual-band[13], and tri-band designs[14,15], as well as rigid and flexible designs. The authors of these studies have aimed to address previously unaddressed challenges to enhance the reliability and functionality of wearable antennas.

Circular Polarization (CP) is a crucial aspect in the design of antennas, as it offers several advantages, including improvements in signal quality, reducing interference, enhancing communication performance, and providing reliable and efficient wireless communication for various healthcare purposes[16–18]. The design of wearable antennas with CP involves various techniques and structures that improve the performance of medical device telemetry systems and address challenges, including multipath interference[19].

The design considerations for circularly polarized antennas in medical device applications include impedance bandwidth, Axial Ratio (AR) bandwidth, biological compatibility, radiation characteristics, and safety. In medical device applications, the size of the antenna holds significant importance. A smaller antenna is preferred because it enhances patient comfort. However, researchers have encountered a significant challenge in reducing the antenna size while maintaining good antenna specifications[20]. In the literature, multiple techniques have been employed to minimize the physical dimensions of antennas, such as using substrates with high dielectric constants and implementing shorting pins[21].

Inserting a shorting pin between the patch and ground planes increases the effective size of the antenna and can reduce its physical dimensions for a given operating frequency. By employing the shorting pin technique, the antenna can be miniaturized to an appropriate size at a specific frequency for applications in this domain[22,23].

Medical device applications require increased gain to maintain reliable communication and signal strength, particularly in the complex and lossy environment surrounding the human body. Additionally, an array topology allows for better control over the radiation pattern. This directional control can help reduce interference and focus the radiation on specific areas of interest resulting in more efficient power consumption and enhanced communication reliability for medical device applications, essential for patient monitoring and data transmission Moreover, the sequential phased feed network used in the array contributes to maintaining the purity of circular polarization. An advantage of circular polarization in Body Area Network (BAN) applications is that it mitigates the effects of multipath propagation and polarization mismatch, which are common challenges in both on-body and in-body communication applications. In terms of scalability and flexibility, there is a high degree of scalability and flexibility in the design of array topologies. Even though our current design consists of four elements, the approach can be scaled to include more elements if higher gain or different radiation characteristics are required. The scalability of single antennas is generally more limited and frequently restricted by their fundamental design constraints[11,24].

Although designing array antennas with rotated elements introduces additional complexity compared to arrays without rotation, there are advantages. These advantages include enhancing the symmetry of antenna array radiation characteristics, improving the axial ratio of circular polarization, mitigating fading and signal degradation, improving the signal-to-noise ratio in crowded wireless communication environments, and increasing the gain[25].

Sequential arrays can be designed to be physically compact while maintaining high performance, making them suitable for applications with limited space[26–28]. Additionally, the assessment of Specific Absorption Rate (SAR) and the interaction between wearable antennas and the human body have been investigated, providing insights into the safety and stability of these antennas[29,30].

High-gain directional antennas increase signal strength and coverage in the desired direction, which enhances the communication range and reliability in a particular direction at the expense of the rest of the directions, unlike omnidirectional antennas, where there is no directional preference and the gain is zero (isotropic). As the antenna size decreases, it becomes electrically small, and the gain decreases to negative values.

Electrically small antennas with negative gain can be acceptable in specific applications, such as Implantable Medical Devices (IMD)[31], where compact size is a critical design factor. Compensating for the negative gain can be achieved through high-performance receivers and other advanced signal-processing techniques, allowing for successful deployment in diverse scenarios[19,32].

This work presents a compact wearable array antenna designed for healthcare monitoring and medical device applications, featuring a miniaturized 2×2 configuration of sequential-phase circularly polarized elements operating in the 2.4 GHz ISM band[33]. The array antenna was fed from the feeding network via a 50-ohm coaxial cable to provide sequential phase shifts to the array elements. The results were experimentally validated. The link budget was calculated for a distance of 10 m, and the SAR was thoroughly analyzed.

Figure 1 depicts an application example in a healthcare monitoring scenario where a patient wears the proposed CP array antenna, facilitating the real-time communication of vital signs data with a ceiling base station in a sick room or hospital setting (with a coverage area radius of 4–8 m).

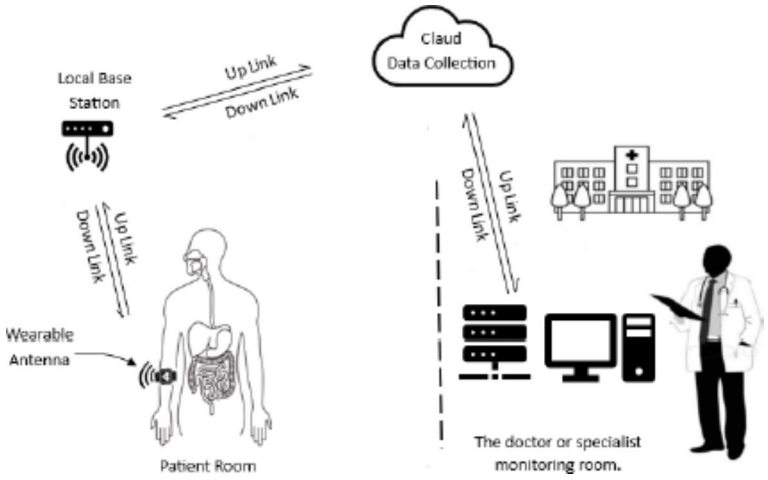

Fig. 1. The proposed antenna application example in a patient room (drawn by the author).

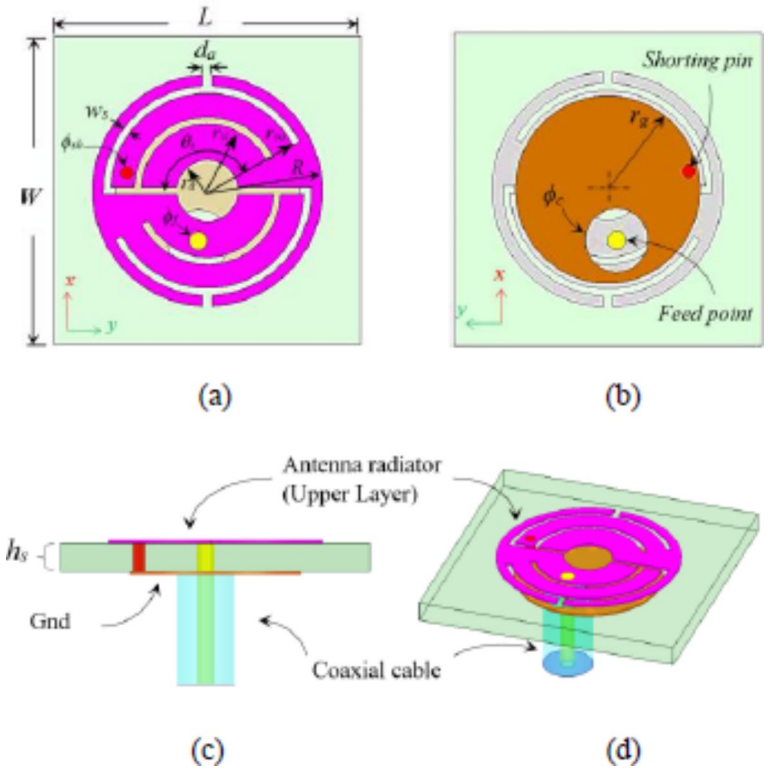

Fig. 2. The geometry of the single antenna element, (**a**) top view (radiator), (**b**) bottom view (ground plane), (**c**) side view (antenna layers), and (**d**) 3D view.

Design methodology

Single antenna design

The proposed antenna element design was created and tested using the (HFSS) software at 2.4 GHz of the ISM frequency band[33,34]. Initially, a single antenna element was designed and optimized using a parametric study procedure to obtain satisfactory performance. Then, the optimized antenna is employed to develop a CP 2 × 2 array antenna. The radiation patch for a single antenna element is characterized by arc-shaped slots in the form of (Ss) distributed symmetrically around the center so that the slot length varies depending on the angle value (θ_s). There is also a circular slot with a radius (r_a) in the center of the radiation patch to control the central frequency (f_c) and impedance value, as shown in Fig. 2. The antenna radius was successfully reduced by incorporating a shorting pin and slots, resulting in impressive miniaturization. A single metal layer is used for the ground plane without requiring additional structures.

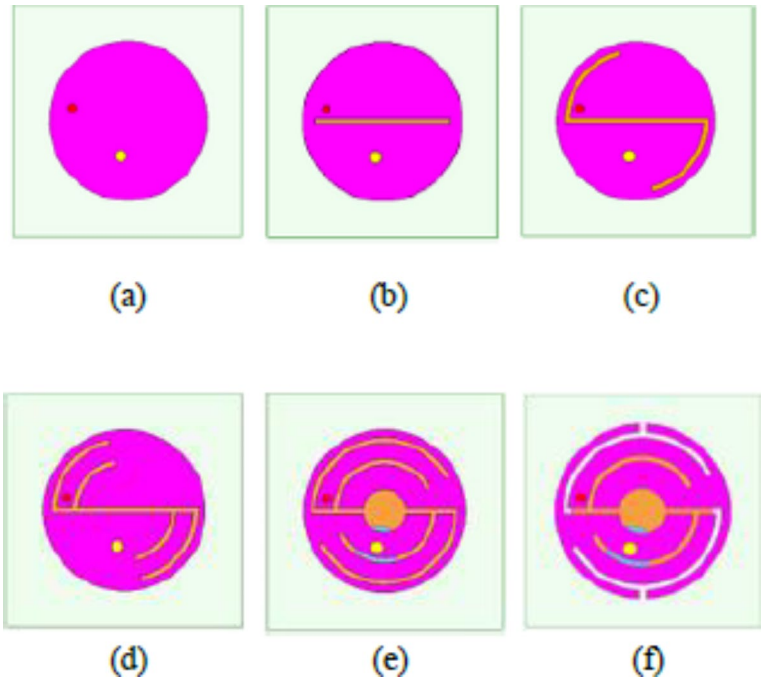

Fig. 3. Antenna structure development steps: (**a**) step 1, (**b**) step 2, (**c**) step 3, (**d**) step 4, (**e**) step 5, and (**f**) step 6.

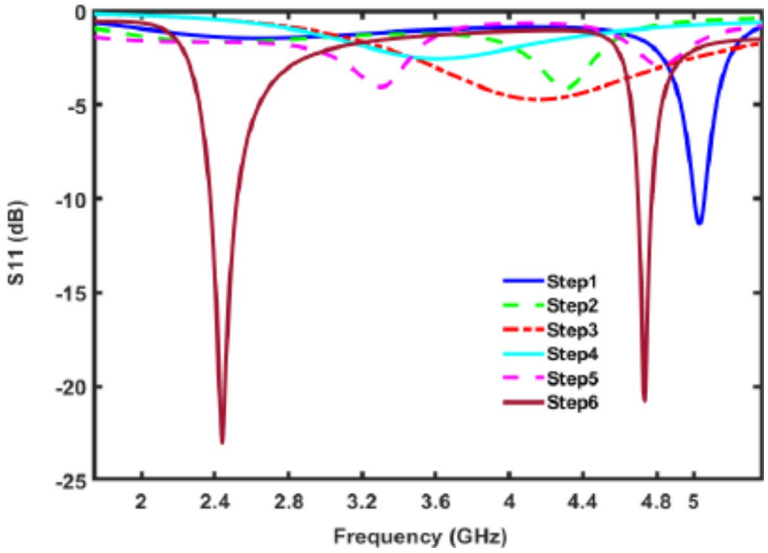

Fig. 4. Variation of the S-parameter considering antenna design steps.

Design structure

The antenna design process passes through six steps, as shown in Fig. 3. Each involves a parameter sweep to examine the antenna response to changes in crucial design parameters. The objective is to determine the optimal parameters for achieving the desired performance metrics and to achieve circular polarization, thereby reducing signal degradation within the human body.

Figure 4 shows the variation of the S-parameter according to the design steps. In Step 1, a conventional patch antenna is powered through a coaxial cable. A shorting pin placed at point (-2.5, 1) helps determine the initial operating frequency of the antenna, which is 5.6 GHz with low impedance matching. In Step 2, adding a slot at the center shifted the resonance frequency slightly lower to 4.4 GHz.

In Step 3, arc slots were created and connected to a central straight slot. Their width (w_{slot}) and length (controlled by θ_s) were adjusted to control the frequency and AR. Adjusting these parameters shifted the antenna resonant frequency to 4.2 GHz but with poor impedance matching. In Step 4, additional symmetrical arc slots

were introduced, causing the resonant frequency to downshift to 3.62 GHz while maintaining poor impedance matching. In Step 5, a variable-radius circular slot was introduced at the center of the antenna to extend the current path and lower the frequency to 3.3 GHz. This adjustment also provided better control over impedance matching through geometric parameters. In Step 6, symmetrical apertures were created between the arc slots and the outward side, with a variable width (w_a) that can be adjusted. These apertures facilitate the antenna resonant frequency and improve the reflection coefficient (S11) and axial ratio (AR) more effectively.

The desired frequency was achieved by adjusting the length and width of the arc slots, the radius of the central circular slot, and the locations of the shorting and feeding pins through a parametric study.

Parametric study

A shorting pin with a diameter ($\phi_{sh} = 0.5$ mm) is positioned at point (x_{sh}, y_{sh}) to reduce the resonant frequency, as shown in Fig. 2. The antenna is excited by a 50 Ω coaxial cable with a core diameter of ($\phi_f = 0.35$ mm) at the feed point at (x_f, y_f). Circular polarization is obtained by precisely adjusting the feeding and shorting pin locations. In addition to changing the dimensions of the other parameters, such as the width (w_s) and length of the arc slots (represented by θ_s) and the diameter of the circular slot on the patch in the middle of the radiation patch (r_a) through an optimization procedure that considers the practical design constraints and leads to the optimal antenna geometry parameters listed in Table 1. The type and thickness of the insulating substrate also affect the antenna resonant frequency. FR4 substrate ($\varepsilon_r = 4.4$ and $\tan\delta = 0.02$) with a thickness of ($h_s = 1$ mm) was selected for the proposed antenna.

A parametric analysis was conducted to evaluate the influence of tuning elements on the performance of the proposed antenna. As demonstrated in Fig. 5(a), modifying the parameter (w_s) significantly influences the impedance bandwidth, enabling the adjustment of the frequency towards the desired location, with an optimal value of 0.25 mm, yielding a good S11< -10 dB performance. Figure 5(b) illustrates the influence of varying the length of the arc slots via (θ_s), which significantly impacts the impedance bandwidth and operating frequency. impedance bandwidth and operating frequency. The optimal value of (θ_s) for achieving effective impedance bandwidth is 150 degrees. Figure 5(c) shows the effects of varying the ground plane radius (r_g) on the (S11) parameter and bandwidth characteristics, with the optimal value of ($r_g = 3.6$ mm). The impact of changing the radius (R) of the antenna radiator element on the (S11) parameter is shown in Fig. 5(d), with the optimal radiator element radius for effective impedance bandwidth ($R = 4.5$ mm).

Modifying the feed point location (x_f, y_f) alters the antenna axial ratio, as depicted in Fig. 5(e). The optimal feed point location is ($x_f = -0.4$), which achieves circular polarization. Figure 5(f) demonstrates the impact of varying the diameter of the central circular slot r_a on the actual maximum antenna gain, indicating that the maximum gain is achieved when r_a equals 1.2 mm. Additionally, Fig. 5(g) illustrates that the axial ratio is influenced by the radius of the central circular slot r_a, with the most favorable axial ratio obtained when r_a is 1.2 mm. It is worth noting that the antenna radiation pattern of the proposed single antenna element is not significantly influenced by the parametric analysis mentioned.

After miniaturizing the single antenna element using shorting pin and slot techniques, improvements were made to the design parameters to improve the antenna characteristics and realize the circular polarization performance of the antenna to have an axial ratio value of less than 3 dB. The CP performance and impedance bandwidth are improved by introducing an additional pair of symmetrical slots with width (d_a). The final dimensions and sizes of the antenna design are shown in Table 1.

Figure 6 shows that the impedance bandwidth achieved at (|S11| < -10 dB) is 140 MHz ranging from 2.37 to 2.51 GHz. Additionally, the AR bandwidth measured for (AR < 3 dB) is 190 MHz. The total volume of the single antenna element obtained is 13 mm × 13 mm × 1 mm, while the area of the radiating patch is only $\pi \times 4.8$ mm^2.

The surface current vector at different phase angles over one period is depicted in Fig. 7. If (T) denotes the wave period from phase degree ($\theta = 0^o$ to 360^o), then, at a phase angle of 0^o ($t = 0$), the principal current vector direction is at $+45^o$. When the phase advances to 90^o (t = $T/4$), the primary current vector is directed toward the $-45°$. At a phase of 180° ($t = T/2$), the primary current vector aligns with the $-135°$ direction. Finally, at a phase of 270° ($t = 3T/4$), the primary current vector points toward the $+135^o$ direction.

Based on the current flow direction depicted on the antenna surface in Fig. 7, it is evident that the circularly polarized antenna emits RHCP waves in the Z direction.

Parameter	Value (mm)	Parameter	Value (mm)
L	13	h_s	1
W	13	θ_s	150 (deg)
R	4.5	ϕ_{sh}	0.5
r_{si}	2.6	ϕ_f	0.7
r_{so}	3.875	ϕ_c	1.223
r_a	1.2	w_s	0.25
d_a	0.2	r_g	3.6
x_{sh}	0.7	x_f	−2
y_{sh}	−3.2	y_f	−0.4

Table 1. Single antenna parameter values.

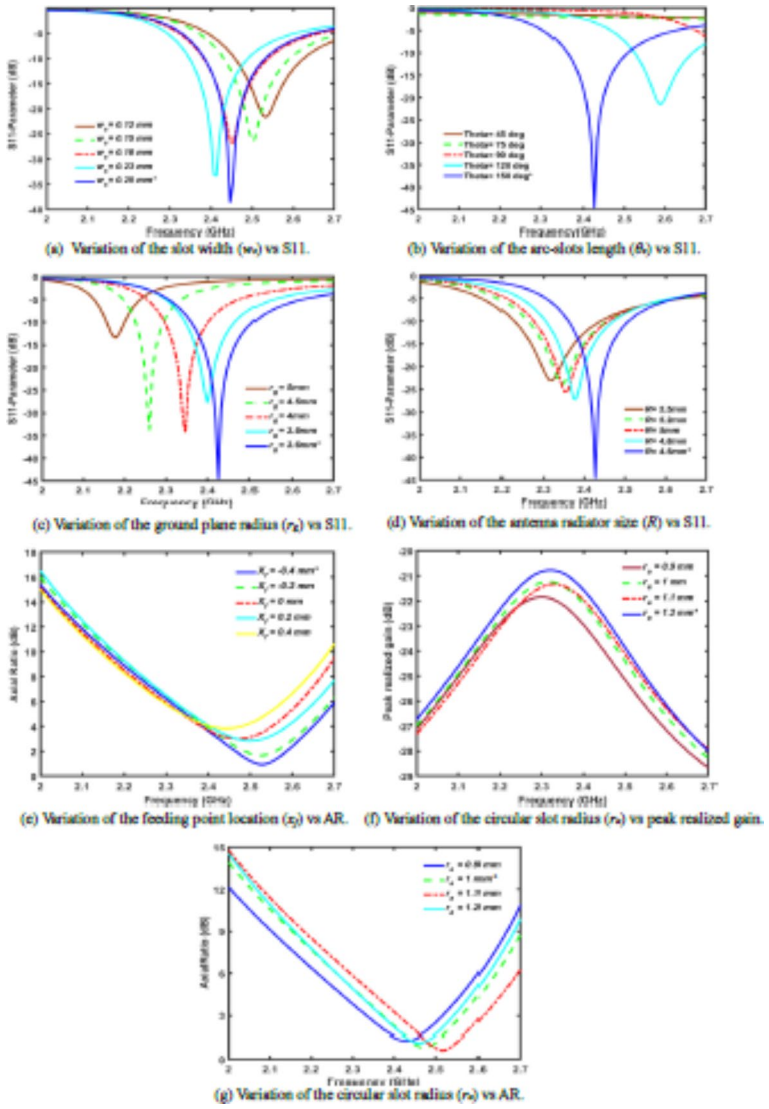

Fig. 5. The parametric response analysis shows the parameters controlling the proposed antenna's performance metrics.

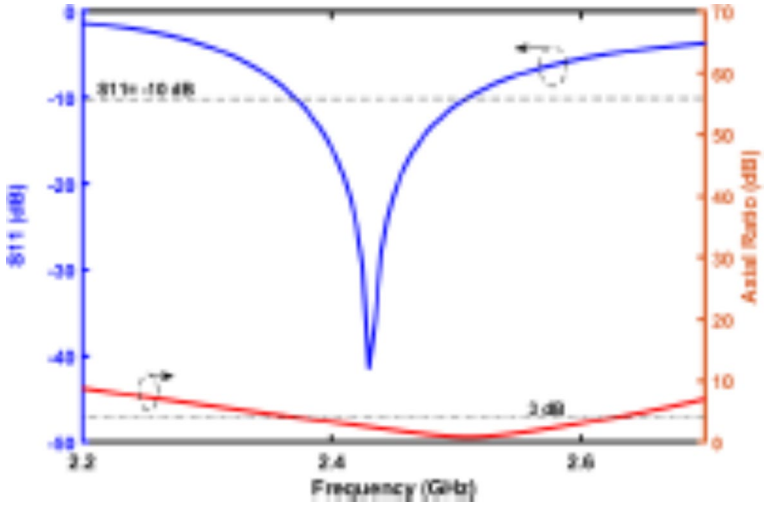

Fig. 6. Simulated S11 and AR bandwidth of the single antenna element.

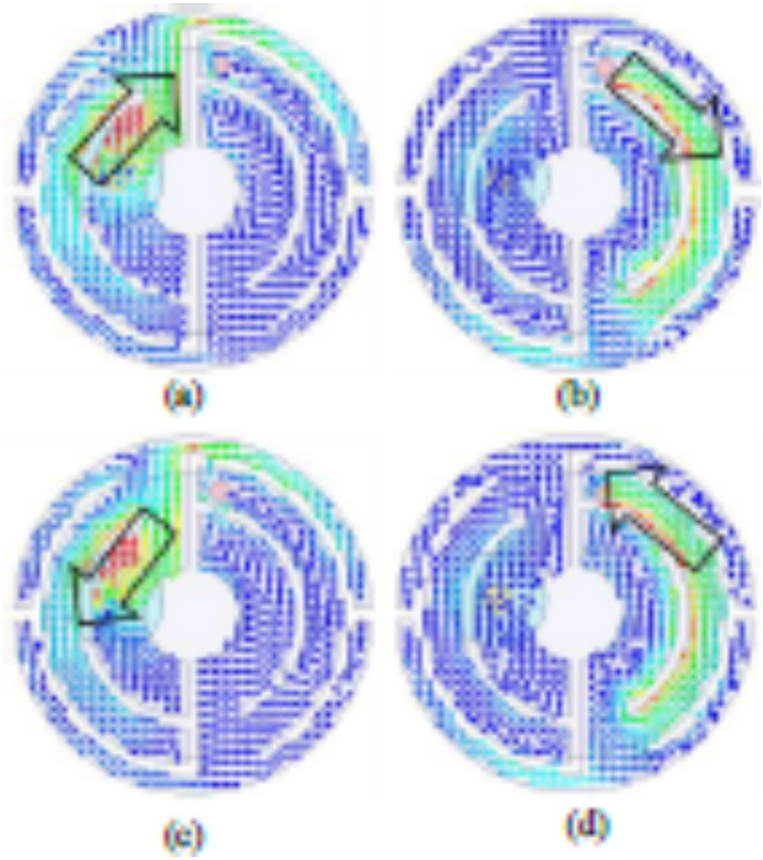

Fig. 7. The current vector distribution: (**a**) at $t=0$, (**b**) at $t=T/4$, (**c**) at $t=T/2$, (**d**) at $t=3T/4$.

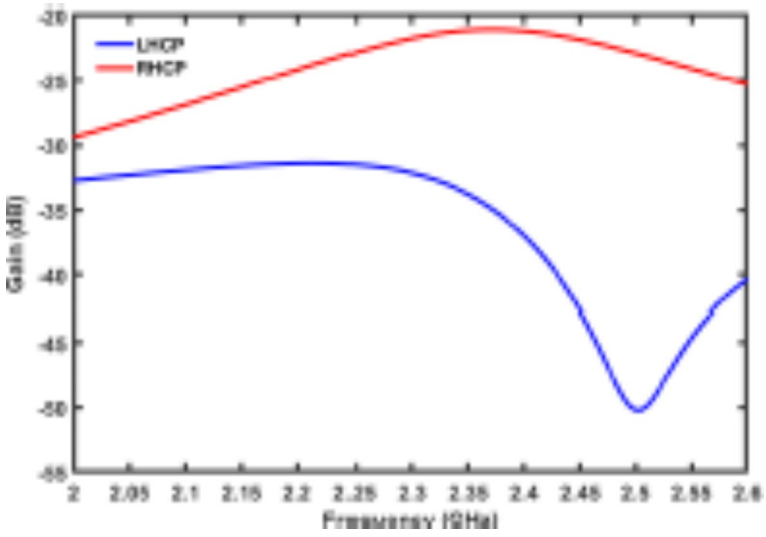

Fig. 8. Simulated RHCP/LHCP gains of the proposed antenna.

The simulated results in Fig. 8 reveal that the proposed antenna achieves a right-hand circular polarization gain (RHCP) of -21 dB, whereas the left-hand circular polarization gain (LHCP) is 40.98 dB at 2.43 GHz, demonstrating its effectiveness in wireless communication. Furthermore, the LHCP and RHCP radiation patterns in Fig. 9 illustrate that the proposed antenna exhibits quasi-omnidirectional radiation.

These results emphasize the validity and suitability of the antenna element for integrating into an array antenna, making it appropriate for use in medical devices that require seamless communication regardless of their orientation.

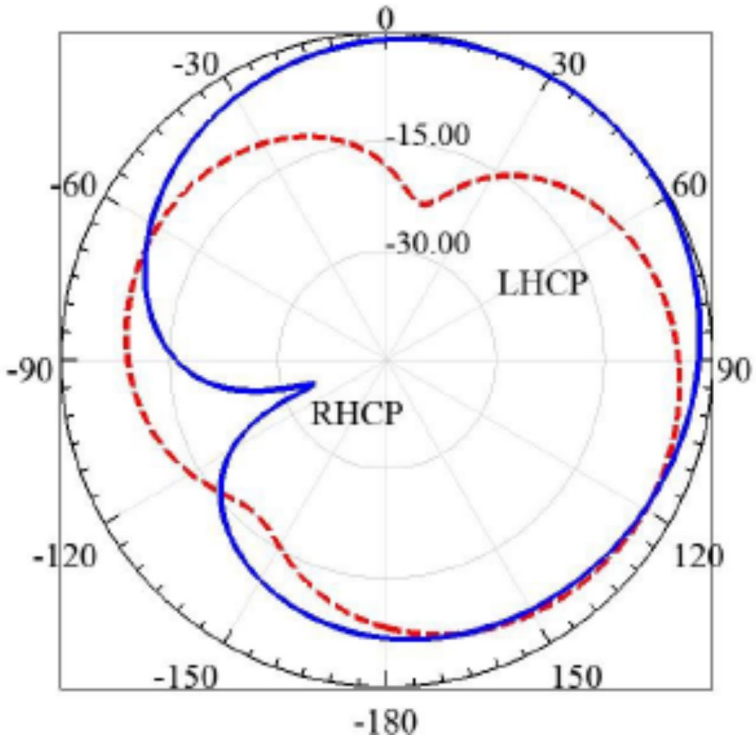

Fig. 9. Simulated normalized RHCP/LHCP radiation patterns of the proposed single antenna at 2.4 GHz frequency.

Feeding network

The feeding network plays a critical role in controlling the phase and amplitude of each antenna element excitation. It is important to note that the feeding network design should be precisely tuned to the 2.4 GHz ISM frequency band. Proper design considerations include the lengths and characteristics of transmission lines, substrate materials, and component dimensions to ensure optimal performance within this frequency range[18,35]. The objective may be achieved using the rat-race and branch-line couplers, optimized for the 2.4 GHz frequency band. The design equations of the rat-race and branch-line couplers can be found in detail in reference[32].

Rat-race coupler

The rat-race coupler, also known as a 3dB hybrid coupler, consists of four ports of $50\sqrt{2}\ \Omega$, each placed at a distance of $(\lambda/4)$ from the other around the top half of the ring with 50 Ω impedance. The length of the bottom half of the ring is $(3\lambda/4)$, and its impedance is $50\sqrt{2}\ \Omega$. Figure 10 shows that it has three branches that are 90-degree phase shifted from each other, and one branch provides a 270-degree phase shift. As a result, it can efficiently split the input signal into two equal amplitude signals while maintaining a 180-degree phase difference between them. The phase difference between the two output ports can be used to achieve circular polarization in the antenna array.

If an input signal is fed into port 1, two output signals with equal amplitude and a 180-degree phase difference are produced at ports 2 and 4, while port 3 remains isolated.

Branch-line coupler

The branch-line coupler provides a balanced power division with a 90-degree phase difference between its output ports[18]. By strategically adjusting the lengths of the transmission lines within the branch-line coupler, the relative phase and amplitude of each antenna element excitation can be controlled [36]. Figure 11 shows the branch-line coupler of the proposed feeding network at a frequency of 2.4 GHz.

A branch-line coupler (or hybrid coupler) aims to achieve a specific coupling factor and phase difference between two output ports. Thus, the equivalent circuit consists of four quarter-wavelength transmission lines organized in a rectangular arrangement. Since the circuitry is entirely planar, the branch-line coupler is the simplest type of quadrature coupler. Each transmission line has a wavelength of one-quarter. Alternative wavelengths such as 3/4, 5/4, or 7/4 may also be used in each arm if the circuit layout necessitates it, though this reduces bandwidth. As a signal enters the top left port, it is split into two quadrature signals on the right (ports 2 and 3), while port 4 is fully isolated from the input port at the center frequency. Since the lower output port (port 3) has the longest path to travel, it has the most negative transmission phase. Generally, branch-line couplers are 3dB, four-port directional couplers having a 90°-phase difference between their output ports, referred to as 'through' and 'coupled' arms. The branch-line coupler (also referred to as the quadrature hybrid) is usually

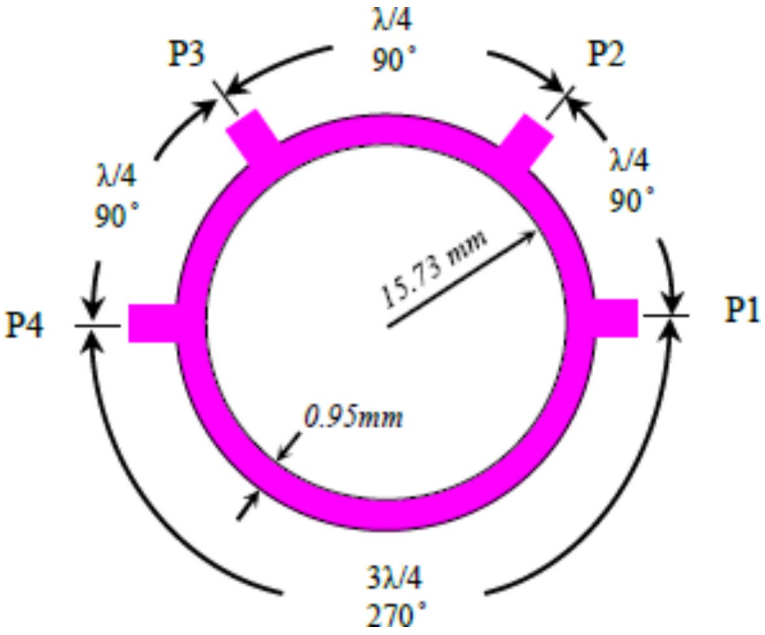

Fig. 10. The rat-race coupler geometry.

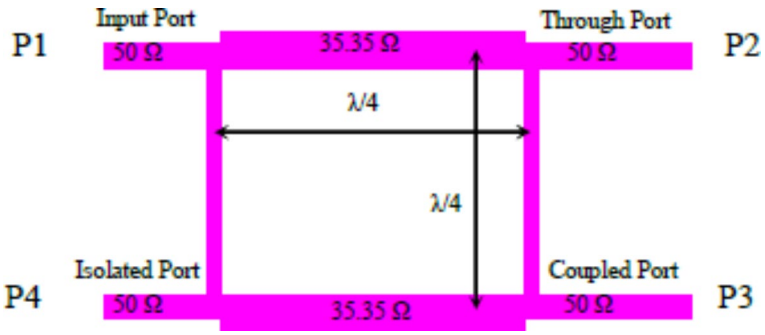

Fig. 11. The branch-line coupler geometry.

fabricated in the form of a microstrip or stripline configuration. The key design equations for a 3-dB branch-line coupler are:

$$Z_1 = Z_0\sqrt{\frac{P_a/P_b}{1+P_a/P_b}} \tag{1}$$

$$Z_2 = Z_0\sqrt{P_a/P_b} \tag{2}$$

where Z0 is the characteristic impedance (50 Ω), P_a is the power output of port 2, P_b is the power output port 3, and Z1, Z2 are the branch output impedances. In this study, the P_a/P_b equals 1, and as a result, the branch output impedances are:

$$Z_1 = Z_0/\sqrt{2} \tag{3}$$

$$Z_2 = Z_0 \tag{4}$$

The compact and efficient design of coupler-based feeding networks is well-suited for integration into wearable devices, contributing to efficient and adaptable wearable technology. Figure 12 shows the configuration of the proposed cascade feeding network consisting of the rat-race coupler and the branch-line coupler built on FR4 substrate material of 110 mm × 95 mm× 0.8 mm.

This configuration allows precise control over the phase and amplitude of the signals delivered to each antenna element. The specific arrangement and parameters of the couplers in the proposed feeding network would achieve the design goals and requirements of the array antenna. The cascade configuration offers the

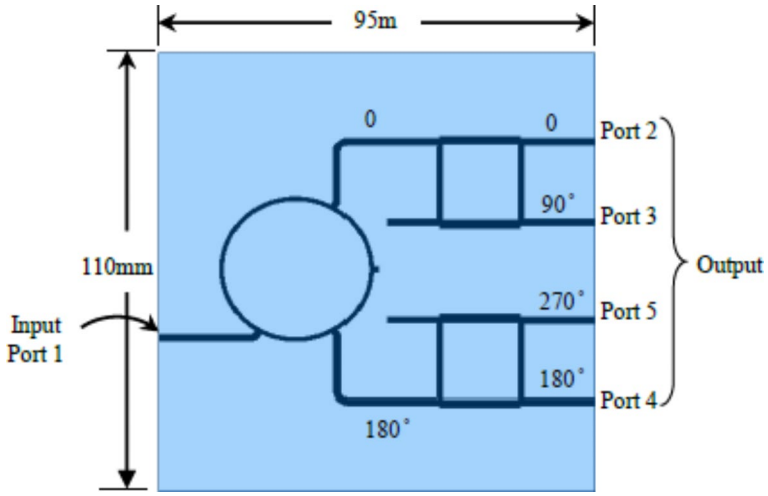

Fig. 12. The proposed feeding network configuration.

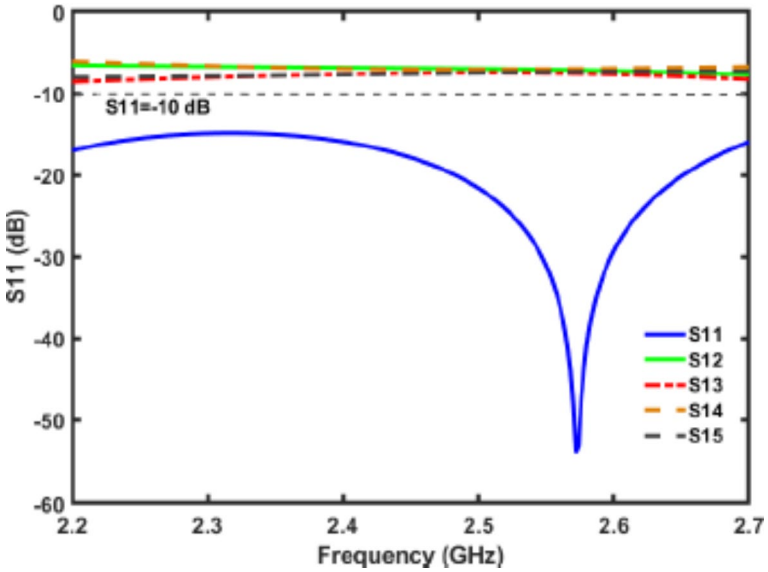

Fig. 13. The reflection coefficient simulation results for the feeding network.

advantages of improved power division and phase control, which are essential for the efficient functioning of the feeding network in wearable devices.

The feeding network is carefully optimized for operation within the 2.4 GHz ISM frequency band involving precise geometric alignment of components, each exhibiting distinct performance attributes, making it an appropriate configuration for the proposed array antenna design. The effect of the feeding network on the performance of the sequential array antenna is crucial and ensures efficient power distribution and phase difference response across the antenna elements.

The simulation results provide valuable insights into the impedance-matching proficiency of the network by visualizing the S-parameters at the feeding port. The results demonstrate a noteworthy impedance bandwidth of 1 GHz, ranging from 1.9 GHz to 2.9 GHz. This finding underscores the feeding network's remarkable capacity for effective impedance matching, demonstrating its capability to cover a broad operating frequency spectrum. The elucidation of these outcomes contributes to a deeper understanding of the feeding network performance and its potential applications in optimizing the functionality of the associated circularly polarized array antenna. Figure 13 presents a comprehensive visualization of the S-parameters observed at the feeding network ports.

The phase responses depicted in Fig. 14 offer a comprehensive insight into the phase difference as a function of frequency. The simulation results indicate an approximate 90-degree phase difference between the output ports, a crucial attribute, particularly in applications dependent on precise phase relationships, such as sequential-phase array antennas. These simulation findings validate the network potential and affirm its suitability for integration into the proposed array antenna design.

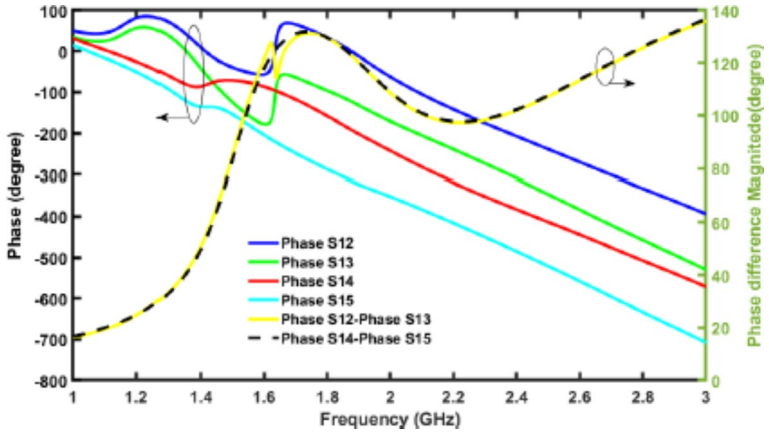

Fig. 14. The simulated phase response of the proposed feeding network.

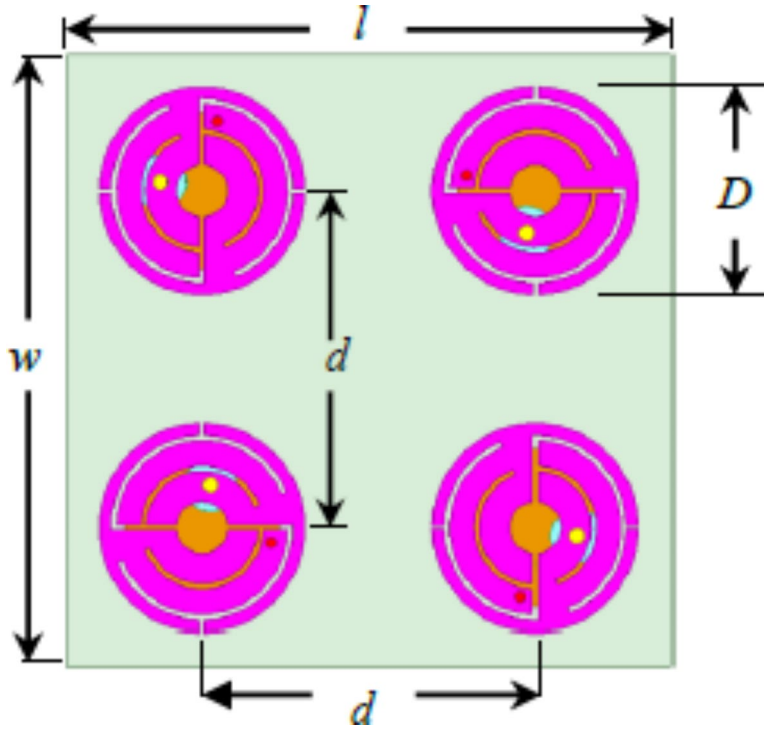

Fig. 15. Geometry of the printed array antenna.

Proposed array antenna structure

The choice of array patch antenna type must correspond to the medical device communication needs, physical constraints, and the desired performance characteristics of the array antenna. Generally, several patch elements are employed in an array configuration to attain beamforming or directional characteristics. As shown in Fig. 15, the proposed array antenna includes four circular-shaped radiation patch antenna elements of diameter (D), a circular ground plane, and a common FR4 substrate of size ($l \times w$) and thickness of (h_s). The construction process is initiated by the sequential positioning of single antenna elements, each with a diameter of $D = 9.6$ mm, along one side of the square FR-4 substrate. The sequential arrangement ensures orthogonal polarization characteristics, which are fundamental for circular polarization. This preliminary configuration provides the foundation for the optimization procedure.

The performance of the feeding network, along with the entire sequentially arranged 2×2 CP antenna array, is validated through comprehensive simulations and practical measurements. Parameters such as impedance matching, axial ratio, radiation patterns, and gain are assessed, demonstrating the effectiveness of the coupler-based feeding network for wearable applications. Through parametric study and adjustments, the antenna elements are resized to the optimal diameter value of ($D = 9$ mm), and the spacing between elements (d_x, d_y)

Parameter	Value (mm)	Parameter	Value (mm)
w	24	l	24
dx	12	dy	12
R	4.5	θ_s	154 (deg)
r_i	2.6	ϕ_{sh}	0.5
r_o	3.8	ϕ_f	0.7
r_a	1.2	ϕ_c	1.223
d_a	0.3	w_s	0.25
h_s	1	r_g	3.6

Table 2. The optimal array antenna geometry parameters.

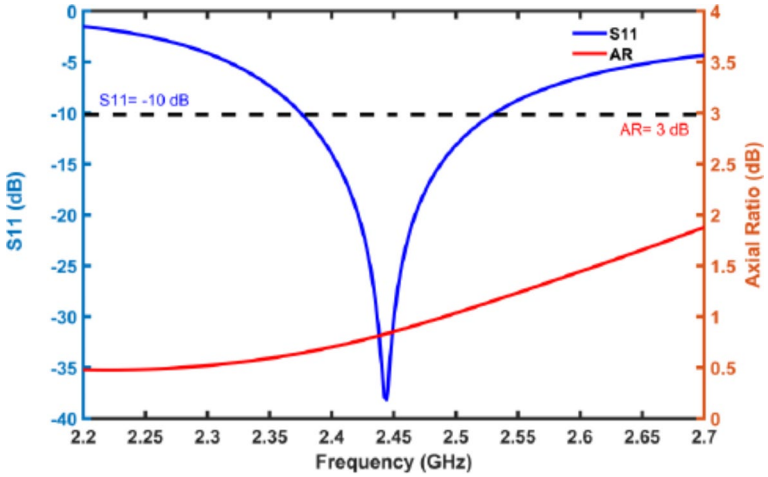

Fig. 16. Simulated S11 and AR bandwidth for Array antenna.

Tissue	Relative permittivity (εr)	Conductivity δ (S/m)
Skin	42.9	1.561
Fat	5.28	0.1028
Muscle	54.48	1.844

Table 3. The Electrical properties of human tissues at 2.4 GHz[37].

is defined as 12 mm. This optimized configuration optimizes the array performance, ensuring high gain and circular polarization purity. The optimal antenna array parameters obtained are listed in Table 2.

Simulating the antenna in HFSS with a biological tissue environment is essential, given its proximity to the body, which can significantly influence antenna performance. This simulation is essential to studying the Specific Absorption Rate (SAR) to ensure compliance with safety standards. A parametric analysis study is employed to determine the optimal parameters for the antenna element, such as diameter, spacing, and configuration. The study aims to analyze the performance characteristics of the array antenna. Figure 16 depicts the simulation results of the array antenna for the reflection coefficient (S11) and the axial ratio (AR). Table 3 lists the electrical properties of human biological tissues[37].

The axial ratio is consistently less than 3 dB, indicating the excellent polarization purity and minimal signal distortion achieved by the novel antenna design under investigation. Figure 17 illustrates that the proposed array antenna achieves a peak realized gain of -14.9 dBi at a frequency of 2.43 GHz, demonstrating that the system superior characteristics are sufficient for a quasi-omnidirectional radiation pattern suitable for sick-room coverage area medical device applications.

The simulation results for the array antenna at the operating frequency of 2.43 GHz reveal an RHCP peak gain of -14.9 dB and an LHCP peak gain of -39.9 dB. Although the sign of the gain value is negative, these results demonstrate excellent performance in signal radiation and input power utilization. Figure 22 shows the simulated and measured gains, validating the antenna efficiency at the specified frequency.

Figure 18 illustrates the simulated normalized cross-polarization gain patterns of the antenna. The patterns demonstrate a comparison of the cross-polarization levels at various angles, providing insights into the antenna's effectiveness in maintaining the desired polarization state across the range of operation.

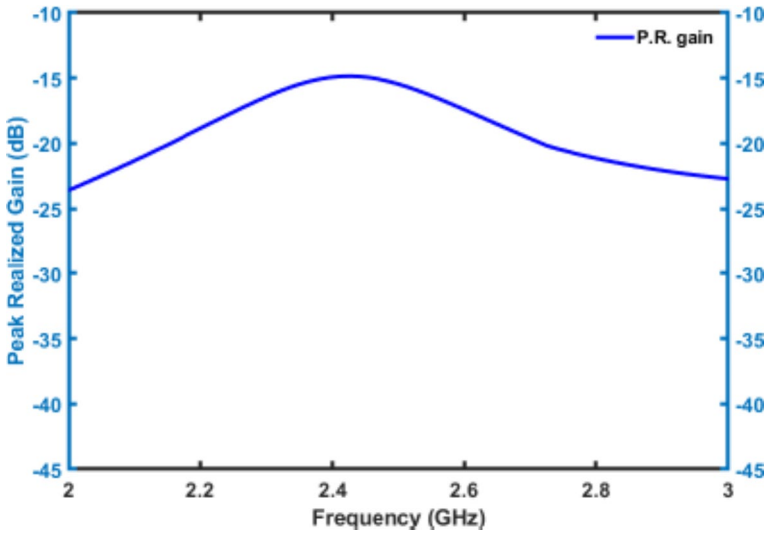

Fig. 17. The simulated peak realized gain of the proposed array.

The simulated gain patterns for RHCP and LHCP of the array antenna are presented in Fig. 23. The results confirm that the proposed array antenna exhibits symmetrical radiation patterns, ensuring uniform coverage and enhancing link quality. This characteristic is crucial for medical devices that demand stable and continuous communication.

The significant difference between LHCP and RHCP gain is mainly due to the design and orientation of the antenna elements and the feed network. The proposed antenna is designed explicitly for RHCP radiation, so the RHCP gain is significantly higher than the LHCP gain. This design choice ensures that the antenna radiates most of its power in the desired RHCP mode, thereby minimizing multipath effects and polarization mismatches in the intended applications for medical devices. Negative values for both LHCP and RHCP gain indicate that the antenna radiates less power in those directions than an isotropic radiator (with a gain of 0 dB). In the context of the design, the RHCP gain of -21 dBic (single element) and − 15 dBic (array) reflects the adequate radiated power in the RHCP mode, which, despite being negative, is sufficient for the specific range and operational requirements of the body area networks (BAN).

As a result of their compact size and proximity to the human body, wearable and miniaturized antennas tend to operate at reduced power levels. As the LHCP gain is significantly lower (more negative) than the RHCP gain, the antenna is highly selective in its polarization, effectively suppressing the unwanted LHCP mode. In order to maintain the integrity of RHCP signals and reduce interference from reflections and multipath components, this selectivity is essential. Furthermore, the negative gain values may initially seem concerning. However, they indicate the antenna's relative performance in the specified polarization states. It is important to note that the difference between the LHCP and RHCP gains is critical to demonstrating the antenna's ability to radiate in the intended polarization (RHCP). This characteristic ensures reliable communication in BAN applications, where consistent polarization is essential for signal integrity.

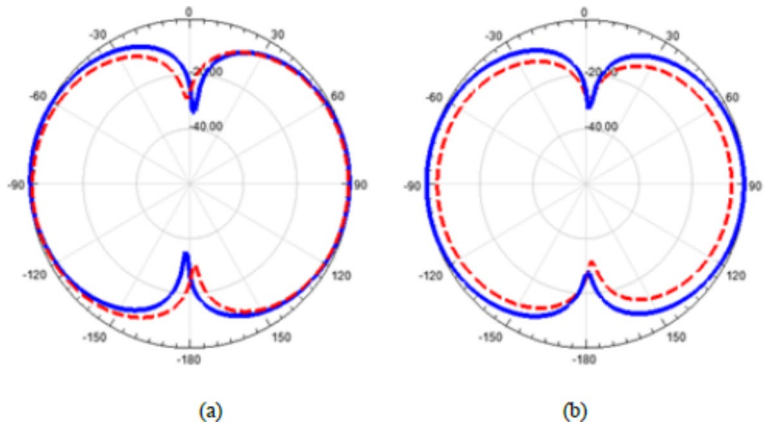

Fig. 18. Simulated normalized (**a**) E-plane and (**b**) H-plane radiation patterns with Co- and Cross-polarization at 2.4 GHz frequency. The solid lines/blue are Co-pol and the dashed lines/red are Cross-pol radiation.

Array antenna fabrication and measurements

Following the simulation process and obtaining satisfactory results, the array antenna and feeding network were fabricated for experimental testing and measurement. Figure 19 shows the fabricated prototypes of the array antenna and feeding network.

Subsequently, an array antenna and feeding network were connected using the standard coaxial cable of appropriate length. Several factors can affect an antenna's performance, including the length of the coaxial cables connecting the feeding network to the array of antenna elements. With increasing length, coaxial cables exhibit an increase in signal loss. The loss is frequency-dependent and is determined by the cable attenuation coefficient (dB/m). In addition to reducing the power delivered to the antenna elements, longer cables may also result in higher insertion losses, resulting in a reduction in the overall gain of the antenna system. Moreover, the signal phase changes as it travels along the cable. This phase shift results in the electrical length of the cable being directly proportional to the operating frequency and the cable length. When cable lengths are not equal, phase mismatches may occur between antenna elements, adversely affecting the antenna performance and polarization purity. It is also possible for variations in cable length to affect the impedance matching between the antenna elements and the feeding network. Impedance matching is essential to minimize reflection losses and ensure efficient power transfer. Mismatched cables can generate standing waves and degrade performance due to reflections. The following strategies were implemented to minimize the adverse effects of cable length on the performance of our antenna:

a) A high-quality, low-loss coaxial cable is carefully selected to connect the feeding network to the antenna elements. This careful planning and decision-making process ensured that a more significant percentage of the transmitted power reached the antenna elements while minimizing signal attenuation over the length of the cables.
b) Coaxial cables of equal length were used for all connections between the feeding network and the antenna elements to prevent phase mismatches. As a result, the signals at each element are in phase, preserving the array's intended radiation pattern and polarization characteristics.
c) The length of the cables was carefully optimized to balance practical deployment constraints with optimal electrical performance. In addition to providing the necessary flexibility for the physical arrangement of the array elements and feeding network, the lengths selected are sufficiently short to minimize loss and phase shift.
d) We carefully designed the transition between the feeding network and the coaxial cables to ensure proper impedance matching. This design consideration minimizes reflection losses and efficiently transfers power from the feeding network to the antenna elements.

The design is assembled and subjected to experimental testing; Fig. 20 displays the measurement setup. The simulated and measured values of the S11 parameter and the AR of the proposed array antenna are shown in Fig. 21.

The proposed array antenna has demonstrated an impedance bandwidth of 21.4% (2.2–2.72 GHz) with circular polarization in the entire operating frequency band. Additionally, the antenna boasts a gain of -14.9 dBi and effectively covers the operating frequency at 2.43 GHz within the ISM band. These results demonstrate a strong correlation between the expected and observed impedance-matching characteristics, affirming the reliability and accuracy of the antenna performance design.

Althoug there is agreement between the simulated and measured results, they do not perfectly match due to several contributing factors. The proposed design consists of two parts of the feed network and an array of elements with a coaxial cable connection. Due to manufacturing tolerances, the physical dimensions of the antenna may vary slightly from the designed specifications. Also, antenna performance can be affected by variations in substrate thickness, dielectric constant, and conductor dimensions. Additionally, connections between the feeding network and the antenna elements, such as solder joints and coaxial connectors, may introduce impedance mismatches and additional losses not accounted for in simulations. However, the environment in which the measurements are conducted, including the antenna's proximity to metallic objects or other sources of interference, can affect the results. In contrast, simulations are typically performed in an idealized environment in which interference is not present.

Figure 22 shows that the measured values of the LHCP gain and RHCP gain closely align with and validate simulation results, demonstrating a strong agreement between the anticipated and observed performance of the array. This agreement between simulation and measurement enhances the credibility of the findings, implying that the theoretical expectations accurately represent the real-world behavior of the antenna. this close correspondence reinforces the overall reliability and confidence in the reported results.

The gain performance of a small wearable antenna demonstrates slightly positive RHCP gain and negative LHCP gain at lower frequencies, with negative gain in the targeted band. This behavior is influenced by the antenna's compact size and proximity to the human body, which causes signal absorption and detuning. The small size limits the antenna efficiency and bandwidth, while the design may prioritize factors like flexibility and wearability over high gain. Although the lower gain, the antenna can still provide a quasi-omnidirectional radiation pattern and maintain good impedance matching, which is suitable for specific wearable applications where consistent coverage and compact design are of greater importance than maximizing gain.

The measured and simulated RHCP and LHCP radiation patterns of the proposed array antenna at a frequency of 2.43 GHz are illustrated in Fig. 23. The experimental results demonstrate that the radiation patterns exhibit stability and agreement with the simulated results. This confirms the antenna's expected characteristics and reliability. The results indicate that the antenna is capable of performing as anticipated. Simulated and measured RHCP/LHCP radiation patterns of the proposed array antenna at 2.43 GHz.

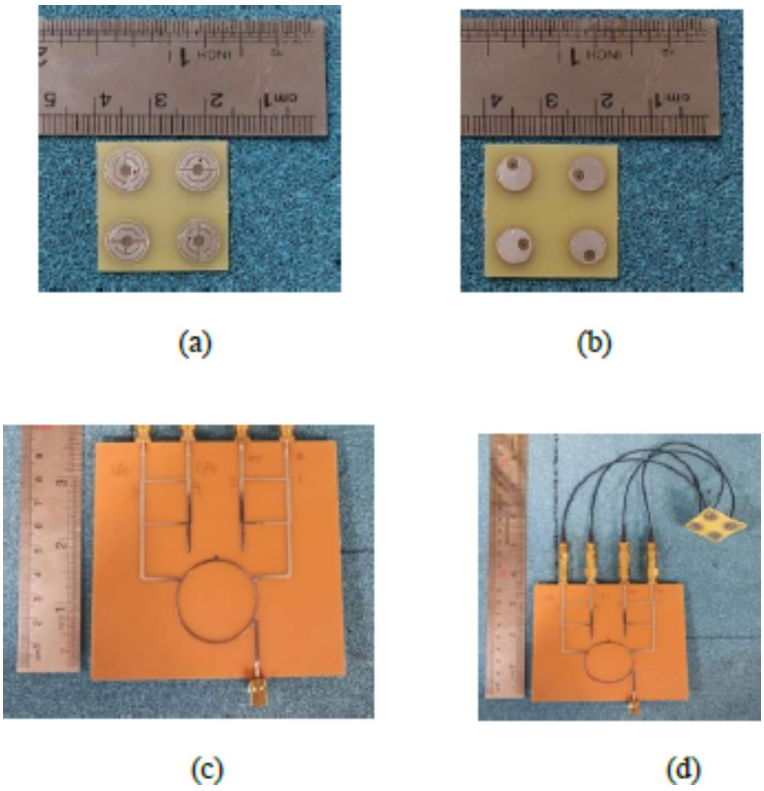

Fig. 19. Fabricated prototype photograph: (**a**) Array antenna top view, (**b**) Array antenna bottom view, (**c**) Feeding network, (**d**) Array antenna connected to the feeding network.

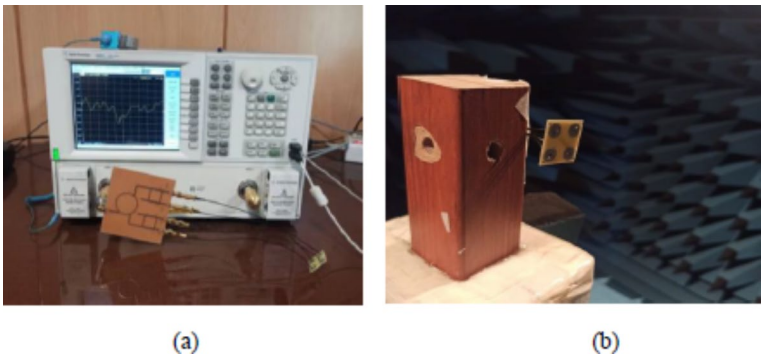

Fig. 20. Measurement setup, (**a**) antenna connected to the network analyzer, and (**b**) antenna placed in an anechoic chamber.

Communication link and sar analysis

The Link Budget assessment is a critical aspect of designing and assessing the performance of the proposed Circularly Polarized (CP) antenna array. The Link Budget provides a comprehensive signal path analysis, considering gains, losses, and other factors to determine the overall communication system performance. The proposed CP array antenna helps mitigate path loss by providing increased gain.

Link margin

The link margin provides crucial insights into the feasibility and reliability of the proposed CP array antenna for the intended communication application. It represents the surplus signal power beyond the minimum requirement for communication. Defined as the difference between the designed received power value and the minimum required threshold at the receiver. The link margin for various communication scenarios can be determined using the Friis transmission equation with the free-space path loss Eq. 3[2]. Table 4 includes all the parameters required to calculate the communication link margin.

The link Margin equation is typically represented as follows:

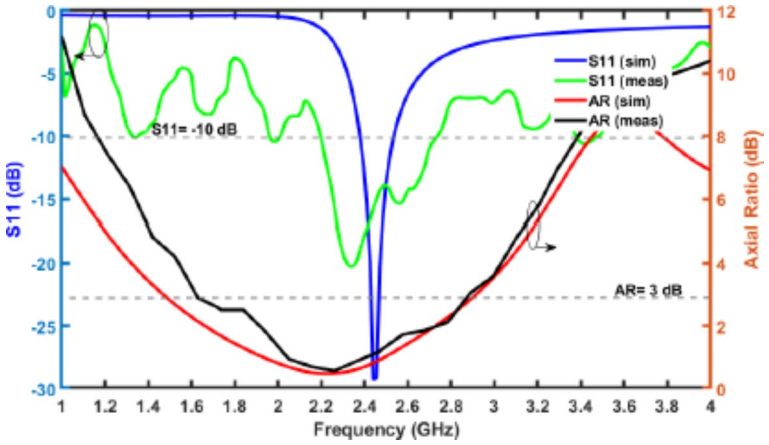

Fig. 21. Simulated and measured impedance and AR bandwidths of the proposed array antenna.

$$L.M. = CNR_{design} - CNR_{thr} \tag{5}$$

$$CNR_{design} = P_t + G_t + G_r - P_{Loss} - N_0 \tag{6}$$

$$CNR_{thr} = E_b/N_0 + 10log_{10}(Be_{rate}) - G_c + G_d \tag{7}$$

$$N_0 = 10\,log_{10}K + 10\,log_{10}T \tag{8}$$

$$T = T_0(NF - 1) \tag{9}$$

where (CNR_{design}) represents the carrier-to-noise ratio when the antenna transmits at a specific power and distance from another antenna, and (CNR_{thre}) is the threshold carrier-to-noise ratio to meet particular criteria of bit-rate (B_r) and bit-error-rate (Be_{rate}) associated with receiver sensitivity. P_r and P_t are the received and transmitted power at the receiver and transmitter, respectively (dBm). G_t and G_r are the gain of the transmitting receiving antenna, respectively (dBi), K is Boltzmann constant (1.38×10^{-23}), T and T_0 are the additional noise temperature introduced by the component and the ambient temperature, respectively (in Kelvin).

The free space path loss formula can be determined from Eq. (10):

$$P_{Loss} = 20\log_{10}(4\pi\, d/\lambda) \tag{10}$$

Using the Shannon-Hartley theorem in (11), the channel capacity is calculated as 1.771 Gbps under ideal conditions, considering an achieved CP impedance bandwidth of 520 MHz and a signal-to-noise ratio for binary phase shift keying (E_b/N_0) of 9.6.

$$C = BW \times log_2(1 + SNR) \tag{11}$$

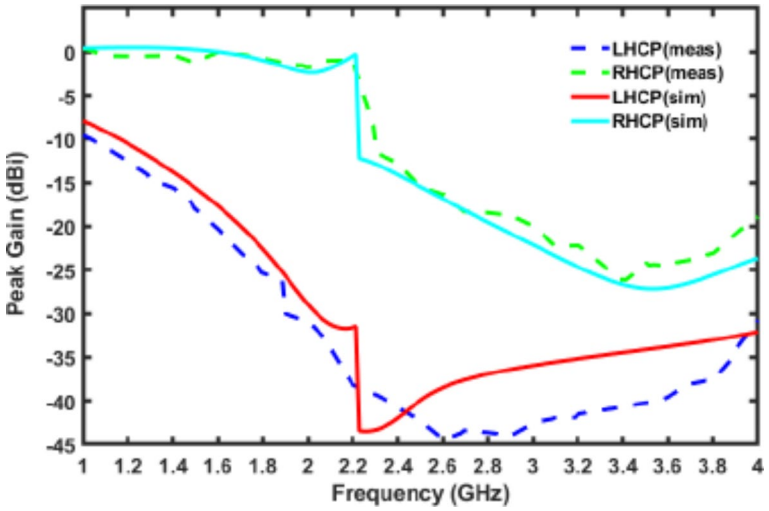

Fig. 22. Simulated and measured RHCP/LHCP gains of the proposed array antenna.

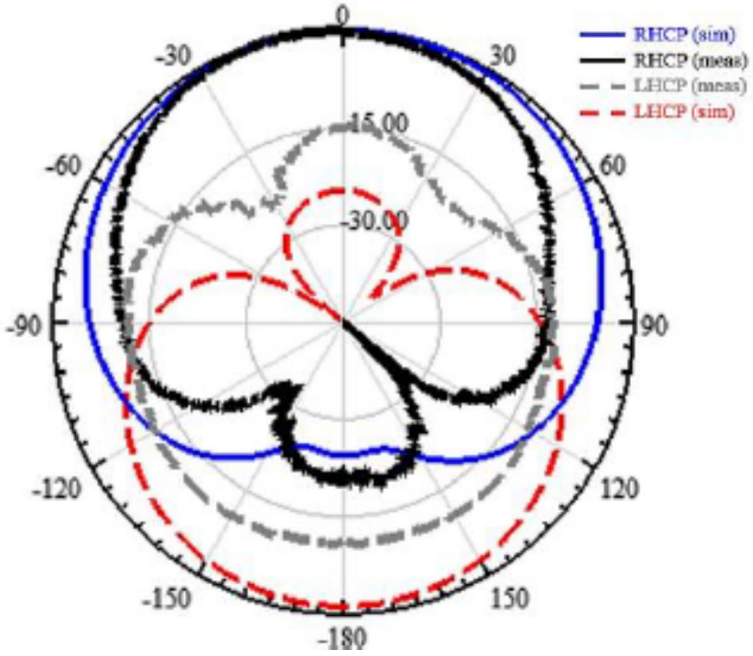

Fig. 23. Simulated and measured RHCP/LHCP radiation patterns of the proposed array antenna at 2.4 GHz frequency.

Parameter	Value
Transmitter	
Operating frequency	2.45 GHz
Polarization	CP
Tx power P_t (dBm)	19.23
Tx antenna gain G_t (dBi)	− 15
Receiver	
Rx antenna Gain G_r (dBi)	2.15
Ambient temperature T_0 (K)	398.2
Receiver noise Fig. NF (dB)	3
Noise power density (dB/Hz)	− 199.95
Signal	
Bite rate B_r (Mb/s)	10
Bite error rate (B_{rate})	1×10^{-5}
E_b/N_0 (ideal BPSK) (dB)	9.6
Coding gain Gc(dB)	0
Fixing deterioration Gd (dB)	2.5

Table 4. Communication link budget parameters.

here ($SNR = E_b/N_0$).

Figure 24 shows that a link margin of 64 dB was achieved with a bit rate transmission of 10 Mb/s at a distance of 10 m. This substantial link margin ensures reliable communication for the proposed antenna, ensuring effective operation within the range of the external monitoring device.

SAR analysis

The safety limit of the proposed antenna is paramount, and it undergoes evaluation using a specific absorption rate (SAR). To comply with the safety standards of IEEE C95.1-1999, SAR levels must be maintained below 1.6 W/kg, typically averaged over 1 g of human tissue. The simulation model incorporates three layers of biological tissues (skin, fat, and muscle). The feeding network represents a power transmission line to the antenna without radiating elements and may influence SAR values by altering power distribution, adding simulation complexity, and providing shielding effects. For these reasons, the SAR analysis often focuses on the wearable array antenna alone to ensure conservative safety estimates and regulatory compliance.

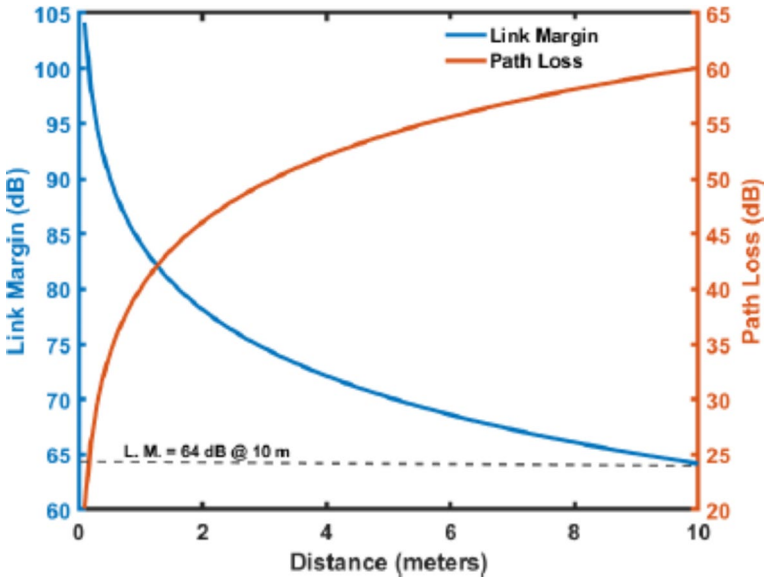

Fig. 24. Link budget analysis at 2.4 GHz and bit rate 10 Mb/s.

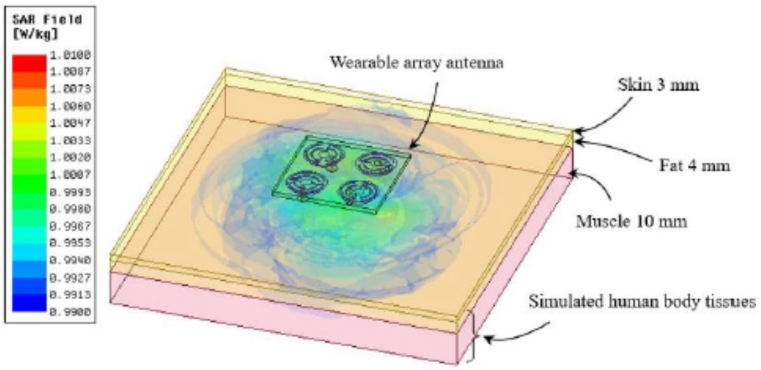

Fig. 25. SAR of the proposed antenna in the simulation model at 2.4 GHz.

Figure 25 depicts the antenna SAR within a simulation model at the operating frequency of 2.45 GHz. The maximum averaged SAR at an input power of 1 W was determined to be 1.01 W/kg; this value aligns with the IEEE C95.1-1999 standard, which sets a SAR limit of 1.6 W/kg.

Table 5 provides a detailed features comparison of the proposed CP array antenna with the researchers' works for wearable antennas in the last decade. The data presented in the table demonstrates the excellent performance of the proposed array antenna in terms of design, size, and functionality compared to prior works in the field.

Conclusion

A compact and novel design of a circularly polarized wearable 2 × 2 array antenna, measuring 24 mm × 24 mm × 1 mm, operating at 2.4 GHz within the ISM band, has been presented. The antenna utilizes a cascade feeding network comprising rat-race and branch-line couplers. The overall size of the array antenna with its feeding network is 110 mm × 95 mm × 1.8 mm. The antenna was fabricated, and the experimental results corresponded with the simulation results. The results indicate that the proposed antenna has an impedance bandwidth of 21.24% and a large AR bandwidth encompassing the entire operating frequency range. The link budget and channel capacity were calculated, yielding a link margin of 64 dB at a bit rate of 10 Mb/s over a coverage area radius of 10 m. This result indicates that the antenna demonstrates effective performance within a patient room. The SAR of the antenna was analyzed, and it complies with the safety limits of IEEE C95.1-1999 standards. The array antenna exhibits excellent impedance matching, gain pattern, and circular polarization capability. This demonstrates the antenna reliability for wireless communication and data transmission between on-body medical devices and remote base stations.

Refs.	Type	Size	f_0 (GHz)	− 10 dB > Impedance BW	Gain dB	Polarization	Overlapping AR BW	SAR (W/kg)	
								1 g	10 g
[38]	Single^F	$(50^2\times\pi\times3)$ mm^3 $(1.98/2\,\lambda_0)^2\times\pi\times0.058\,\lambda_0$	5.8	8.1%	− 0.55	Linear	–	1.21	–
[39]	Single^R	$(15^2\times\pi\times7.5)$ mm^3 $(0.0917/2\,\lambda_0)^2\times\pi\times0.0229\,\lambda_0$	0.9175	0.54%	− 5.6	Linear	–	–	–
[40]	Single^R	$(55\times55\times5)$ mm^3 $0.44\,\lambda_0\times0.44\,\lambda_0\times0.04\,\lambda_0$	2.4	4.5%	3.5	CP	2.4%	0.54	–
[41]	Single^F	$(65\times54\times1.2)$ mm^3 $0.531\,\lambda_0\times0.441\,\lambda_0\times0.009\,\lambda_0$	2.4	40.4%	− 7	Linear	–	0.368	–
[42]	Single^R	$(13.77\times12.99\times14.44)$ mm^3 $0.226\,\lambda_0\times0.251\,\lambda_0\times0.28\,\lambda_0$	5.8	18.9%	6.22	CP	18.3%	0.182	0.106
[43]	Single^F	$(39\times39\times0.508)$ mm^3 $0.318\,\lambda_0\times0.318\,\lambda_0\times0.004\,\lambda_0$	2.4	7.75%	− 0.57	Linear	–	1.7	2.1
[44]	Single^F	$(35.17\times35.17\times2.275)$ mm^3 $0.68\,\lambda_0\times0.68\,\lambda_0\times0.044\,\lambda_0$	5.8	6.6%	7.2	CP	3.85%	–	0.294
[45]	Array^F	$(321\times61\times6)$ mm^3 $58.85\,\lambda_0\times1.118\,\lambda_0\times0.11\,\lambda_0$	5.5	45.6%	2.6	CP	21.1%	0.174	–
[16]	Single^F	$(130\times130\times3.34)$ mm^3 $1.04\,\lambda_0\times1.04\,\lambda_0\times0.027\,\lambda_0$	2.4	18%	8.9	CP	14.3%	–	0.059
This work	Array^R	$(110\times95\times1.8)$ mm^3 $0.88\,\lambda_0\times0.76\,\lambda_0\times0.0144\,\lambda_0$	2.4	21.24%	− 13.9	CP	21.24%	1.01	–

Table 5. Comparison of the proposed CP array antenna characteristics with another wearable antenna works. R : Rigged substrate, F : Flexible substrate.

Data availability

The datasets used and/or analysed during the current study available from the corresponding author on reasonable request by email (ch.ghobadi@urmia.ac.ir).

Received: 6 May 2024; Accepted: 27 September 2024
Published online: 29 October 2024

References

1. Srinath, B. S. P., Jammalamadaka, K., Hindodi, A. & A. & Advancement of existing healthcare setting through tele-medicine: The challenges faced in India. *Int. J. Community Med. Public. Health*. **8**, 502 (2020).
2. Nikita & Konstantina *Handbook of Biomedical Telemetry*. (2014).
3. Omran, M. M., Mutashar, S. & Ezzulddin, A. Design of an (8×8) mm2 efficient inductive power link for medical applications. in *2nd International Conference on Engineering Technology and its Applications, IICETA 2019* 61–66 (Institute of Electrical and Electronics Engineers Inc., 2019). https://doi.org/10.1109/IICETA47481.2019.9012992
4. Babaei, N., Hannani, N., Dabanloo, N. J. & Bahadori, S. A. Systematic review of the use of commercial wearable activity trackers for monitoring recovery in individuals undergoing total hip replacement surgery. *Cyborg. Bionic Syst*. (2022). https://doi.org/10.34133/2022/9794641
5. Ali, S. M. et al. Recent advances of wearable antennas in materials, fabrication methods, designs, and their applications: State-of-the-art. *Micromachines*. (2020). https://doi.org/10.3390/mi11100888
6. Hashim, F. F., Mahadi, W. N. L. B., Latef, A., Bin, T. & Othman, M. Bin. Key factors in the implementation of wearable antennas for WBNs and ISM applications: A review WBNs and ISM applications: A review. *Electronics (Switzerland)*. (2022). https://doi.org/10.3390/electronics11152470
7. Wang, F. *Assembly Conformal Antenna Array for Wearable Microwave Breast Imaging Application*. (2017).
8. Farooq, U., Iftikhar, A., Khan, M. S., Shafique, M. F. & Shubair, R. M. *Design of a 1×4 CPW Microstrip Antenna Array on PET Substrate for Biomedical Applications*. (2019).
9. Januszkiewicz, Ł., Di Barba, P. & Hausman, S. Optimal design of switchable wearable antenna array for wireless sensor networks. *Sens. (Switzerland)*. **20**, (2020).
10. Zu, H., Wu, B., Yang, P., Li, W. & Liu, J. Wideband and high-gain wearable antenna array with specific absorption rate suppression. *Electron. (Switzerland)*. **10**, (2021).
11. Kumar Malik, P., Naim, A. & Singh, R. *Printed Antennas; Design and Challenges*.
12. Peddakrishna, S., Wang, L., Kollipara, V. & Kumar, J. Compact circularly polarized monopole antenna using characteristic mode analysis. in *Proceedings of Engineering and Technology Innovation*, vol. **20**.
13. Awan, W. A., Islam, T., Alsunaydih, F. N., Alsaleem, F. & Alhassoonc, K. Dual-band MIMO antenna with low mutual coupling for 2.4/5.8 GHz communication and wearable technologies. *PLoS One*. **19**, (2024).
14. Awan, W. A. et al. A conformal tri-band antenna for flexible devices and body-centric wireless communications. *Micromachines (Basel)*. **14**, (2023).
15. Bairappaka, S. K., Ghosh, A., Kumar, J. & Bhattacharya, A. A compact triple band circular polarized slotted microstrip patch antenna with low frequency ratio. *Int. J. RF Microwave Comput. Aided Eng.* **32**, (2022).
16. Chen, Z. et al. Enhancing circular polarization performance of low-profile patch antennas for wearables using characteristic mode analysis. *Sensors*. **23**, (2023).
17. Siahcheshm, A., Nourinia, J. & Ghobadi, C. Circularly polarized antenna array with a new sequential phase feed network utilizing directional coupler. *AEU - Int. J. Electron. Commun.* **93**, 75–82 (2018).
18. Shokri, M., Ghobadi, C. & Nourinia, J. Dual-band circularly polarized asymmetric dipole array antenna for GPS L1 and L2 bands. *AEU - Int. J. Electron. Commun.* **169**, (2023).
19. Gao, S., Luo, Q. & Zhu, F. *Circularly Polarized Antennas* (2014).
20. Kiourti, A. & Nikita, K. S. Miniature scalp-implantable antennas for telemetry in the MICS and ISM bands: Design, safety considerations and link budget analysis. *IEEE Trans. Antennas Propag.* **60**, 3568–3575 (2012).

21. Aliqab, K., Nadeem, I. & Khan, S. R. A comprehensive review of in-body biomedical antennas: Design, challenges and applications. *Micromachines*. (2023). https://doi.org/10.3390/mi14071472
22. Tung, L. V. & Seo, C. A. Miniaturized implantable antenna for wireless power transfer and communication in biomedical applications. *J. Electromagn. Eng. Sci.* **22**, 440–446 (2022).
23. Wu, Y. & Sun, H. A. Low-profile Wideband Omnidirectional Antenna with reconfigurable tri-polarization diversity. *AEU-International J. Electron. Commun.*.
24. Mahfuz, M. M. H. et al. Wearable Textile Patch Antenna: Challenges and future directions. *IEEE Access.* **10**, 38406–38427 (2022).
25. Wang, X., Tong, X., Wang, J., Wang, J. & Han, X. A polarization conversion metasurface for reducing radar cross section and enhancing radiation performance of circularly polarized array antennas. *Opt. Commun*.
26. Li, Q. Q., Pan, H., Zhao, Z. H. & Zhang, H. F. A circularly polarized antenna array with sequential-phase feed network. *J. Electromagn. Waves Appl.* **36**, 1244–1256 (2022).
27. Kuhlmann, K. Sequential rotation of antenna array elements—Rotation Angle for optimum array polarization. *Adv. Radio Sci.* **20**, 17–21 (2023).
28. Wen, C. et al. Slow-time FDA-MIMO technique with application to STAP Radar. *IEEE Trans. Aerosp. Electron. Syst.* **58**, 74–95 (2022).
29. Harris, L. O. SAR computation for multiple wearable antennas. in *Progress In Electromagnetic Research Symposium (PIERS)* (2016).
30. Atanasov, N. T. et al. Wearable antennas for Sensor Networks and IoT applications: evaluation of SAR and Biological effects. *Sensors* **22**, (2022).
31. Malik, N. A., Sant, P., Ajmal, T. & Ur-Rehman, M. Implantable antennas for Bio-medical Applications. *IEEE J. Electromagn. RF Microw. Med. Biol.* **5**, 84–96 (2021).
32. Pozar, D. M. *Microwave Engineering-Wiley (2012)* (Wiley, 2012).
33. Mahn, T. G., Washington, C., Barritt, K. A. & Washington, P. *Navigating Government Regulation in the New Medical Age*. www.fr.com. (2017).
34. FCC-06-103A1.
35. Siahcheshm, A., Nourinia, J., Ghobadi, C., Karamirad, M. & Mohammadi, B. A broadband circularly polarized cavity-backed archimedean spiral array antenna for C-band applications. *AEU - Int. J. Electron. Commun.* **81**, 218–226 (2017).
36. Pourbagher, M., Nourinia, J. & Ghobadi, C. Circularly polarized printed crossed-dipole antenna using branch-line feed network for GPS applications. *AEU - Int. J. Electron. Commun.* **120**, (2020).
37. Air, U. S. Body Tissue Dielectric Parameters _ Federal Communications Commission_2.4GHz.
38. Tak, J., Hong, Y. & Choi, J. Textile antenna with EBG structure for body surface wave enhancement. *Electron. Lett.* **51**, 1131–1132 (2015).
39. Liu, Q., Le, T., He, S. & Tentzeris, M. M. Button-shaped radio-frequency identification tag combining three-dimensional and inkjet printing technologies. *IET Microwaves Antennas Propag.* **10**, 737–741 (2016).
40. Jiang, Z. H., Gregory, M. D. & Werner, D. H. Design and experimental investigation of a Compact Circularly Polarized Integrated Filtering Antenna for Wearable Biotelemetric devices. *IEEE Trans. Biomed. Circ. Syst.* **10**, 328–338 (2016).
41. Rizwan, M., Khan, M. W. A., Sydanheimo, L., Virkki, J. & Ukkonen, L. Flexible and stretchable brush-painted Wearable Antenna on a three-Dimensional (3-D) printed substrate. *IEEE Antennas Wirel. Propag. Lett.* **16**, 3108–3112 (2017).
42. Ullah, U., Mabrouk, I., Ben & Koziel, S. A. Compact Circularly Polarized Antenna with directional pattern for Wearable off-body communications. *IEEE Antennas Wirel. Propag. Lett.* **18**, 2523–2527 (2019).
43. Arif, A. et al. Low-profile fractal antenna for wearable on-body WBAN applications. *IEEE Antennas Wirel. Propag. Lett.* **18**, 981–985 (2019).
44. Yang, H. C., Liu, X. Y., Fan, Y. & Tentzeris, M. M. Flexible circularly polarized antenna with axial ratio bandwidth enhancement for off-body communications. *IET Microwaves Antennas Propag.* **15**, 754–767 (2020).
45. Yang, H., Liu, X. & Fan, Y. Design of Broadband Circularly Polarized All-Textile Antenna and its conformal array for Wearable devices. *IEEE Trans. Antennas Propag.* **70**, 209–220 (2022).

Author contributions

Muammer Omran studied the conception and design of the work and also wrote the main manuscript text. Changiz Ghobadi and Javad Nourinia prepared an analysis and interpretation of the results from data collection. Majid Shokri prepared test setup and measure the antenna.All authors reviewed the results and approved the final version of the manuscript.

Declarations

Competing interests

The authors declare no competing interests.

Additional information

Correspondence and requests for materials should be addressed to C.G.

Reprints and permissions information is available at www.nature.com/reprints.

Publisher's note Springer Nature remains neutral with regard to jurisdictional claims in published maps and institutional affiliations.